LETTER

doi:10.1038/nature20795

High-spatial-resolution mapping of catalytic reactions on single particles

Chung-Yeh Wu[1,2], William J. Wolf[1,2], Yehonatan Levartovsky[3,4], Hans A. Bechtel[5], Michael C. Martin[5], F. Dean Toste[1,2]* & Elad Gross[3,4]*

The critical role in surface reactions and heterogeneous catalysis of metal atoms with low coordination numbers, such as found at atomic steps and surface defects, is firmly established[1,2]. But despite the growing availability of tools that enable detailed *in situ* characterization[3], so far it has not been possible to document this role directly. Surface properties can be mapped with high spatial resolution, and catalytic conversion can be tracked with a clear chemical signature; however, the combination of the two, which would enable high-spatial-resolution detection of reactions on catalytic surfaces, has rarely been achieved. Single-molecule fluorescence spectroscopy has been used to image and characterize single turnover sites at catalytic surfaces[4,5], but is restricted to reactions that generate highly fluorescing product molecules. Here we map the chemical conversion of N-heterocyclic carbene molecules attached to catalytic particles using synchrotron-radiation-based infrared nanospectroscopy[6,7] with a spatial resolution of 25 nanometres, which enables us to distinguish between particle regions that differ in reactivity. We demonstrate that, compared to the flat regions on top of the particles, the peripheries of the particles—which contain metal atoms with low coordination numbers—are more active in catalysing oxidation and reduction of chemically active groups in surface-anchored N-heterocyclic carbene molecules.

Conventional spectroscopic techniques for *in situ* analysis of catalytic reactions—such as infrared, ultraviolet–visible and Raman spectroscopy—can provide critical insight into the catalytic process, but are limited in their spatial resolution to the micrometre scale[8,9]. Near-field microscopy approaches can overcome such diffraction limitations by spatially confining light–matter interactions. In scanning near-field optical microscopy, for example, a metallic atomic force microscope (AFM) tip effectively acts as an optical antenna by localizing and scattering incident light in the near-field region of its apex (Fig. 1a)[10–12]. Consequently, the spatial resolution of scanning near-field optical microscopy is determined by the diameter of the tip apex, which is typically less than 25 nm (ref. 13). Tip-enhanced Raman spectroscopy (TERS) and infrared nanospectroscopy are two complementary apertureless approaches that use tip–light interactions to overcome the diffraction limit of light and to detect the vibrational spectrum of molecules on surfaces with high spatial resolution[10,13]. TERS measurements can also identify time-resolved processes with a temporal resolution of a few seconds on thermally stable substrates[12,14].

Synchrotron-radiation-based infrared nanospectroscopy (SINS) measurements use broad, bright and spatially coherent infrared synchrotron radiation as a source for infrared measurements, which provide intrinsic chemical contrast and spectroscopic identification of a wide range of temperature-sensitive materials[6,7]. Unlike TERS, infrared scattering is a linear phenomenon and is therefore less affected by changes in the tip structure[15], providing reproducible, minimally invasive, high-spatial-resolution spectroscopic analysis of solids[16], polymers[17,18] and proteins[19].

Real-time detection of catalytic reactions at the nanoscale with SINS measurements is currently not possible because the typical durations of the reactions (<1 s) are much shorter than the acquisition time of a single-point infrared spectrum; but differences in reactivity can be mapped spatially using chemically active, surface-anchored N-heterocyclic carbene molecules (NHCs) as model reactants. NHCs were functionalized with a hydroxyl group and anchored to the surface of platinum (Pt) particles[20–23] (Fig. 1a) so that the functional groups reside in close proximity to catalytically active sites and can be oxidized and subsequently reduced upon exposure to oxidizing and reducing conditions (Fig. 1b). These chemical changes are recorded with high-spatial-resolution SINS measurements to reveal differences in activity between different surface sites.

Pt particles with an average size of 100 ± 30 nm were prepared by annealing a Pt film deposited on silicon (Si) surface[20]. NHCs with a chemically active hydroxyl group were chemically anchored to the supported Pt particles (Extended Data Figs 1, 2)[21–23]; the sample was exposed to 1 atm of O_2 at 40 °C for 10 h and then transferred for AFM topography measurements (Fig. 2a). Infrared spectra were collected at selected points along the surface of the sample (marked by coloured circles in Fig. 2b). Measurements with the AFM tip above the bare Si surface and then at the perimeter of the Pt particle (green and red circles in Fig. 2b) yielded a featureless infrared spectrum and a spectrum with few vibrational peaks (green and red spectra in Fig. 2c), respectively. The peaks in the latter spectrum at 1,250 cm^{-1}, 1,800 cm^{-1} and 2,800 cm^{-1} were assigned to C–OH, C=O and O–H vibrations, respectively, and are indicative of hydroxyl-group oxidation to acid and aldehyde in some of the surface-anchored molecules. (The shift of the C=O peak position to relatively high wavenumbers of 1,800 cm^{-1} is due to the close proximity of the functional groups to the metal surface and the close packing of surface-anchored NHCs[24].) The infrared spectrum collected over the centre of the particle (black circle in Fig. 2b) exhibited a dominant peak at 1,250 cm^{-1} and a minor peak at 1,800 cm^{-1} (black curve in Fig. 2c), with the dominant peak associated with C–OH stretch and thus indicating that most of the surface-adsorbed molecules at this site were not oxidized following their exposure to mild oxidizing conditions. Figure 2c also shows an average spectrum (in blue) measured with far-field attenuated total reflectance infrared (ATR-IR) spectroscopy on the same sample, which is seen to represent a linear combination of the two infrared spectra collected in the nanospectroscopy point measurements.

Having established that SINS can map site-dependent differences in reactivity on single particles, infrared nanospectroscopy line scans were conducted following exposure of the sample to various reaction conditions (Fig. 3). The sample was exposed to mild oxidizing conditions (1 atm O_2, 40 °C, 10 h), the topography of the sample was recorded by AFM (Fig. 3a) and then an infrared nanospectroscopy line-scan measurement (marked with a red arrow in the AFM image) was performed along the centre of two adjacent Pt particles (Fig. 3a), revealing a clear correlation between the infrared peak position pattern and the

[1]Department of Chemistry, University of California, Berkeley, California 94720, USA. [2]Chemical Sciences Division, Lawrence Berkeley National Laboratory, 1 Cyclotron Road, Berkeley, California 94720, USA. [3]Institute of Chemistry, The Hebrew University of Jerusalem, Jerusalem 91904, Israel. [4]The Center for Nanoscience and Nanotechnology, The Hebrew University of Jerusalem, Jerusalem 91904, Israel. [5]Advanced Light Source, Lawrence Berkeley National Laboratory, 1 Cyclotron Road, Berkeley, California 94720, USA.

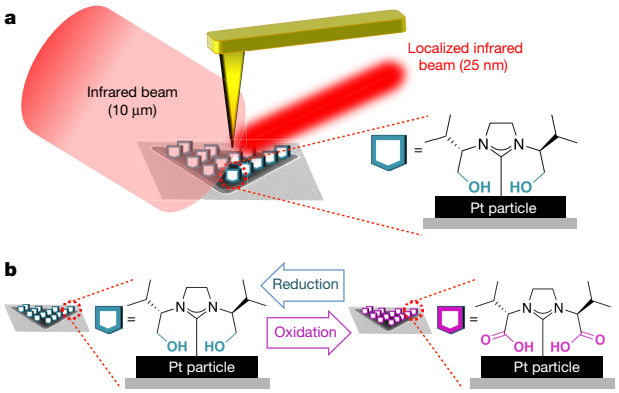

Figure 1 | Schematic representation of the experimental set-up. **a**, OH-functionalized NHCs (blue pentagons) were anchored to the surface of Pt particles (black triangle), which were deposited on a Si wafer (grey surface). A PtSi AFM tip (yellow) acts as an optical antenna by localizing the diffraction-limited synchrotron-sourced infrared beam (which has a diameter of about 10 μm), inducing an infrared scattering signal with a tip-limited spatial resolution of about 25 nm. **b**, Under oxidizing conditions the catalytically active Pt particles oxidize the functional hydroxyl group of the anchored NHCs into acid (purple pentagons). This reaction is reversible and under reducing conditions the acid group can be reduced back into the hydroxyl group (blue pentagons).

topography of the scanned particles. For example, infrared absorption at 1,250 cm^{-1}, which correlates to a C–OH vibration, peaks dominantly at the two locations where Pt particles are detected by AFM (Fig. 3a). The line-scan measurements did not detect C=O vibrations, whereas evidence for O–H stretching appeared at relatively high wavenumbers (3,100–3,250 cm^{-1}). These observations indicate that most of the surface-adsorbed molecules were not oxidized during exposure to mild oxidizing conditions.

The sample was removed from the AFM stage, exposed to harsher oxidizing conditions (1 atm O_2, 70 °C, 10 h) and infrared measurements were performed along the surface of a single Pt particle (Fig. 3b), revealing vibrational peaks at 1,200–1,350 cm^{-1}, 1,750–1,850 cm^{-1} and 2,850–3,250 cm^{-1} assigned to C–OH, C=O and O–H vibrations, respectively. The appearance of C=O stretching vibration and the shift of the OH peak to lower wavenumbers is consistent with oxidation of the OH functional group from alcohol into acid under the harsher conditions used. Interestingly, the amplitude of the C–OH peak did not change, indicating that most of the functional groups of the NHCs were oxidized into the corresponding carboxylic acid. Exposure of the sample to even harsher oxidizing conditions (immersion in aqueous H_2O_2) did not lead to any further changes in the infrared spectra.

The fully oxidized sample was exposed to mild reducing conditions (1 atm H_2, 40 °C, 10 h), with subsequent measurements revealing a decreased C=O vibration amplitude that is consistent with some of the surface-anchored molecules having been reduced (Fig. 3c). Exposure to harsher reducing conditions (1 atm H_2, 70 °C, 10 h) induced further changes in the infrared spectra (Fig. 3d): the C=O vibration could not be detected and the O–H signal was shifted to higher wavenumbers (3,100–3,250 cm^{-1}), indicating that most of the oxidized functional groups had been reduced. Similar changes in the vibration spectra were detected in macroscale ATR-IR measurements (Extended Data Fig. 3).

The influence of isotopic exchange to uncover the mechanism of the reduction process was also studied[25]. Pt-anchored NHCs were exposed to harsh oxidizing conditions (1 atm O_2, 70 °C, 10 h) and then reduced by exposure of the sample to H_2 (1 atm, 70 °C, 10 h). Afterwards, the sample was reoxidized (1 atm O_2, 70 °C, 10 h) and then reduced using D_2 (1 atm, 70 °C, 10 h). Figure 3e, f compares the AFM images and infrared spectra obtained after exposure of the samples to H_2 and D_2, respectively, revealing the appearance of an additional infrared peak at 2,100 cm^{-1} for the sample reduced by D_2, which is attributed to an O–D vibration. Its presence confirms that the reduction of the carboxylic acid group into an alcohol was activated by exposure to D_2. O–H vibrations (about 3,000 cm^{-1}) were still observed for this sample in addition to the O–D vibrations (Fig. 3f), indicating that an H–D exchange reaction had occurred. We propose that hydrogen atoms from the acid functional group interacted with neighbouring NHCs during the reduction process and led to the formation of both –OH- and –OD-functionalized NHCs on the surface.

This approach also enables the correlation between catalytic activity and nanoparticle surface locations, containing surface atoms with different coordination numbers, to be directly probed[26–28]. Because the coordination number of surface atoms that reside along the perimeter of the nanoparticle is lower than that of their counterparts that reside on the flat centre of the particle, and because lower coordination

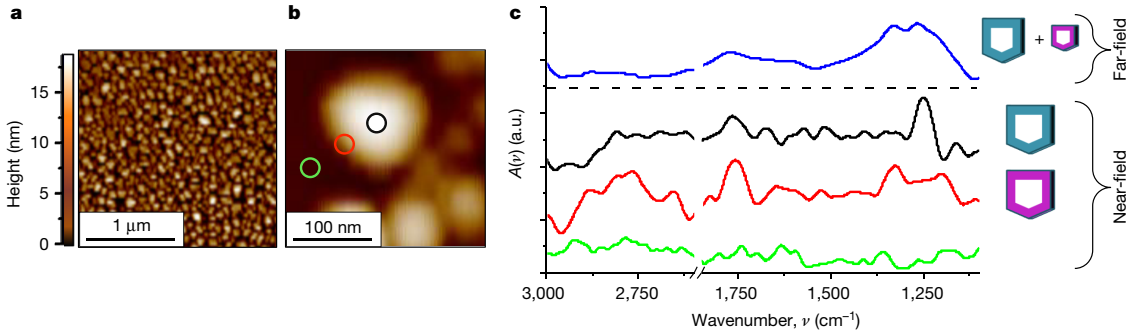

Figure 2 | Comparison between near-field and far-field infrared spectroscopy. **a**, Large-scale topography AFM image of Si-supported Pt particles. The Pt particles were coated with hydroxyl-functionalized NHCs. **b**, **c**, Infrared nanospectroscopy point measurements were conducted on the bare Si surface (green circle in **b** and green infrared spectrum in **c**) and on the edge and centre of a single Pt particle (red and black circles, respectively, in **b** and the correspondingly coloured infrared spectra in **c**). These near-field spectra are reported in the form of a normalized scattering amplitude $A(\nu) = A_{sample}(\nu)/A_{reference}(\nu)$, where ν is the wavenumber, and $A_{sample}(\nu)$ and $A_{reference}(\nu)$ are the scattering near-field amplitudes that were recorded when the AFM tip was located on the NHC-coated particle and on the bare Si surface, respectively. The far-field ATR-IR spectrum of the sample is also shown (**c**; blue spectrum). The spectral range 1,900–2,500 cm^{-1} is excluded in **c**, owing to a diminished signal-to-noise ratio caused by intense infrared absorption by a diamond window, which is part of the synchrotron beamline (Extended Data Fig. 7). The presence of OH-terminated NHCs on the Pt surface is indicated by a blue pentagon and the presence of oxidized NHCs is indicated by a purple pentagon. The relative sizes of the pentagons represent their surface density, as detected by the infrared measurements. The AFM image in **b** is a close-up of the image in **a**. a.u., arbitrary units.

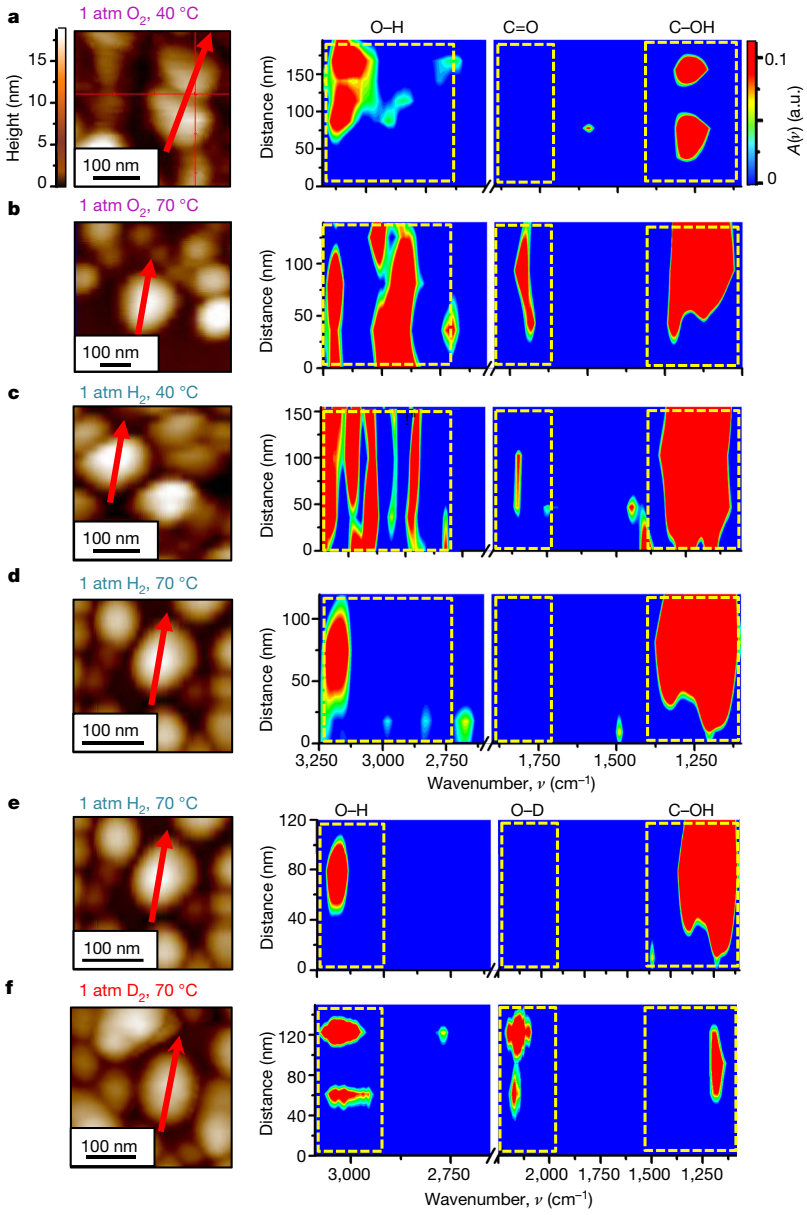

Figure 3 | AFM topography scans and infrared nanospectroscopy line scans. The paths of the infrared line scans along the surface of the sample are marked by red arrows in the AFM images (left column). The colour scale represents the measured height of the Pt particles. The $A(\nu)$ values (colour scale) that were measured during these line scans are shown in the right column. The dashed boxed areas indicate the CO–H, C=O and O–H absorption wavenumbers, highlighting the changes in the infrared spectra in these regions, which are induced by exposure of the sample to various reaction conditions. **a**–**d**, The sample was exposed to oxidizing (**a**, **b**) or reducing conditions (**c**, **d**), as specified, before nanospectroscopy measurements. **e**, **f**, Following exposure of the sample to oxidizing conditions, the sample was exposed to 1 atm of H_2 (**e**) or D_2 (**f**). To bias the lower signal-to-noise ratio in the infrared spectrum at high wavenumbers (>2,600 cm^{-1}), the $A(\nu)$ values in this range were increased by 25% (non-biased spectra are presented in Extended Data Fig. 8). The presence of OH-terminated and oxidized NHCs is indicated by blue and purple pentagons, respectively. The relative sizes of the pentagons represent their surface density, as detected by the infrared measurements.

number is associated with lower activation energy for bond cleavage[29], we performed infrared line scans across the centre and edge of the same particles (Fig. 4). The infrared spectra in Fig. 4a were obtained after exposure to mild oxidizing conditions (1 atm O_2, 40 °C, 10 h) and scanning over two adjacent particles (marked by red and green arrows, respectively, in Fig. 4a); the top and bottom spectra were obtained from measurements performed along the centre and edge of the particles, respectively. Similarities in the pattern of the two infrared line-scan spectra verified that these scans were performed along the same particles. The presence of the two peaks at 1,820 cm^{-1} and 2,950 cm^{-1} in only the infrared line scan performed across the edge of the particle indicates that NHCs anchored to the perimeter of the particle were oxidized following exposure of the sample to mild oxidizing conditions, whereas their counterparts on the centre of the particle did not react. These results demonstrate that the oxidation process occurred with higher probability (lower activation energy) on the perimeter of the particle than on the centre of the particle (Fig. 4b).

Exposing the sample to harsher oxidizing conditions (1 atm O_2, 70 °C, 10 h) eliminated the differences in the infrared line scans, indicating that both the perimeter- and centre-anchored molecules were fully oxidized. Differences re-appeared when the fully oxidized sample was exposed to mild reducing conditions (1 atm H_2, 40 °C, 10 h) (Fig. 4c): infrared spectra collected at the edge of a Pt particle (green arrow in the AFM topography image and the bottom infrared line scan in Fig. 4c) revealed reduction of the functional group back into alcohol as demonstrated by the absence of a C=O peak and shift of the O–H peak to higher wavenumbers, whereas spectra collected across the centre of the particle (red arrow in the AFM topography image and the top infrared line scan in Fig. 4c) showed that the NHCs did not react upon exposure to mild reducing conditions. The properties of surface-anchored NHCs on different sites of the particle after their exposure to mild reducing conditions is schematically shown in Fig. 4d. The observed differences in the infrared spectra represent position-dependent reactivity that, in analogy with the oxidation experiment in Fig. 4a, could not be resolved

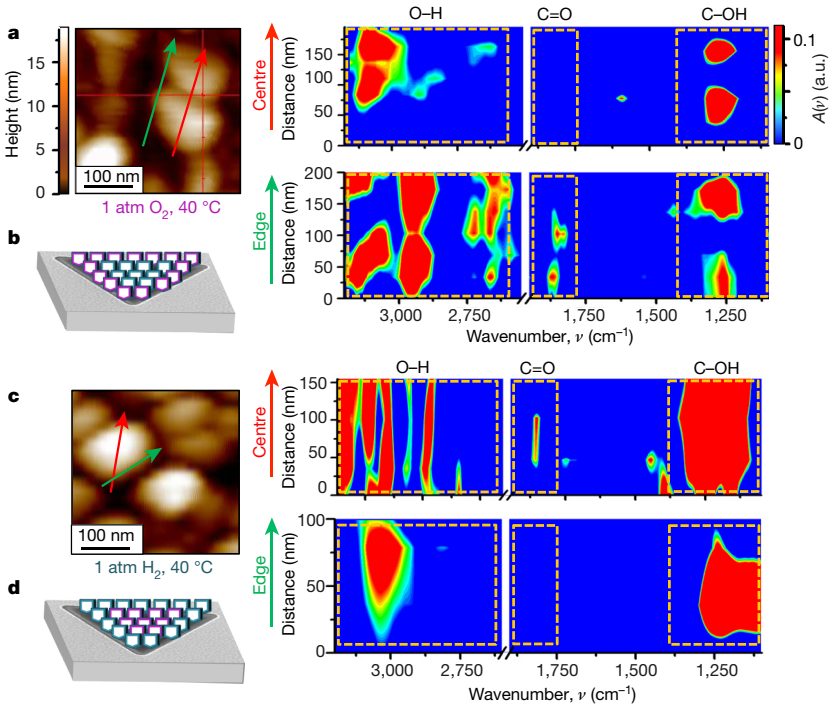

Figure 4 | Infrared nanospectroscopy line-scan measurements on the centre and edge of Pt particles. a, **c**, Infrared nanospectroscopy line scans were performed across the centre and edge of NHC-coated Pt particles (marked by red and green arrows in the AFM images, respectively) following exposure of the sample to mild oxidizing (**a**) and reducing (**c**) conditions. To bias the lower signal-to-noise ratio of the infrared spectra at high wavenumbers (>2,600 cm^{-1}), the $A(\nu)$ values in this range were increased by 25% (non-biased spectra are presented in Extended Data Fig. 9). **b**, **d**, Schematics of NHCs-coated Pt particles after their exposure to reducing (**b**) and oxidizing (**d**) conditions.

once the sample was exposed to harsher reducing conditions (1 atm H_2, 70 °C, 10 h) that induced complete conversion of the functional groups.

To demonstrate the generality of our approach to mapping the catalytic activity on single particles, we studied the reduction of NO_2-functionlized NHCs anchored to the surface of Au particles (Fig. 5a). The related reduction of $-NO_2$ to $-NH_2$ of surface-anchored *p*-nitrothiophenol has previously been studied by tip-enhanced[12,14] and surface-enhanced[30] Raman spectroscopy. Highly crystalline Au particles with an average size of 200 ± 50 nm were prepared on Si surface (Extended Data Fig. 4) and coated with NO_2-functionlized NHCs. Fourier-transform infrared (FTIR) measurements on NO_2-functionlized NHCs in solution, before surface attachment, revealed two main infrared peaks, at 1,355 cm^{-1} and 1,560 cm^{-1} (black spectrum in Fig. 5b). A single-point SINS measurement on an NHC-coated Au particle (location marked by red circle in Fig. 5c) detected two main peaks, at 1,345 cm^{-1} and 1,550 cm^{-1}, that correlate with the symmetric and asymmetric stretches of $-NO_2$, respectively (see red spectrum in Fig. 5b). The high similarity between the macroscale FTIR spectrum of solution-phase NHCs and the nanoscale SINS spectrum of surface-anchored NHCs specifies that neither surface adsorption nor tip-enhanced infrared measurement changed the infrared spectrum

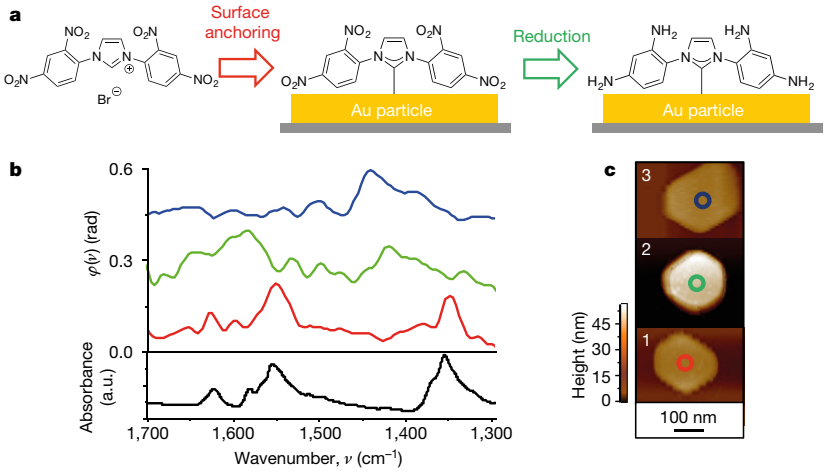

Figure 5 | Infrared nanospectroscopy measurements of NO_2-functionlized NHCs on Au particles. a, Schematic representation of the experimental set-up. **b**, Solution-phase ATR-IR spectrum of inactivated NO_2-functionalized imidazolium salt (black spectrum). Infrared nanospectroscopy point measurements were conducted on single Au particles using the following processes: red, adsorption of NO_2-functionalized NHCs; green, exposure of the sample to a reducing agent ($NaBH_3CN$); blue, exposure of the sample to a deuterated reducing agent ($NaBD_3CN$). The near-field spectra were reported in the form of a normalized scattering phase $\varphi(\nu) = \varphi_{sample}(\nu)/\varphi_{reference}(\nu)$, where $\varphi_{sample}(\nu)$ and $\varphi_{reference}(\nu)$ are the scattering near-field phases that were recorded when the AFM tip was located on the NHC-coated particle and on the bare Si surface, respectively. **c**, AFM topography images showing the locations on the Au particles of the infrared nanospectroscopy point measurements (coloured circles). The colours of the circles correspond to the colours of the spectra in **b**.

of NHCs in a noticeable way. The comparable position of $(N{=}O)_2$ stretches in NO_2-functionalized NHCs (1,345 cm^{-1} and 1,540 cm^{-1}, as detected by SINS) and *p*-nitrothiophenol (1,345 cm^{-1} and 1,570 cm^{-1}, as detected by TERS) demonstrate the complementary nature of these two tip-enhanced apertureless methods.

A single-point SINS measurement of the sample after exposure to reducing conditions (immersion in 0.1 mg ml^{-1} $NaBH_3CN$ in EtOH) detected a peak at 1,420 cm^{-1} and a broader peak at 1,540–1,660 cm^{-1}, which were correlated to C–N stretch and N–H bending, respectively (green spectrum in Fig. 5b, with measurement location indicated by the green circle in Fig. 5c). Although the low signal-to-noise levels of SINS measurements at high wavenumbers (>3,100 cm^{-1}) prevented the detection of N–H stretching vibrations at about 3,400 cm^{-1}, the observed infrared spectral changes indicate that the functional $–NO_2$ groups were reduced to $–NH_2$ following exposure of the sample to reducing conditions, as confirmed by X-ray photoelectron spectroscopy (XPS) measurements (Extended Data Fig. 5). When carrying out the reduction using a deuterated agent (immersion in 0.1 mg ml^{-1} $NaBD_3CN$ in EtOH), the subsequent SINS measurement detected a main infrared peak at 1,435 cm^{-1}, which was related to C–N stretching (blue spectrum in Fig. 5b and blue circle in Fig. 5c). The lack of N–H bending vibration signal in the measured spectrum indicates that the product molecules, whose formation was verified by XPS (Extended Data Fig. 5), were fully deuterated. Low signal-to-noise ratio at lower wavenumbers prevented the expected detection of the N–D vibration at about 1,150 cm^{-1} (Extended Data Fig. 6).

This study has explored how the oxidation and reduction activity of catalysts, towards hydroxyl and nitro functional groups, correlates with particle regions that are characterized by differently coordinated surface atoms (particle perimeter with low-coordination-number surface atoms versus flat surface interior with higher-coordination-number atoms). These observations illustrate the value of the NHC-based strategy, in conjunction with infrared nanospectroscopy, for high-spatial-resolution (approximately 25 nm) mapping of chemical reactions on metallic particles. Using tips with narrower apices (approximately 5 nm) as a way to increase the spatial resolution of SINS measurements is being investigated. Our approach allows the catalytic properties of different surface sites to be determined, enabling a better understanding of heterogeneous catalysts and the design of improved catalysts.

Online Content Methods, along with any additional Extended Data display items and Source Data, are available in the online version of the paper; references unique to these sections appear only in the online paper.

Received 28 June; accepted 11 November 2016.
Published online 11 January 2017.

1. Somorjai, G. A. & Li, Y. *Introduction to Surface Chemistry and Catalysis* 2nd edn (Wiley, 2010).
2. Zambelli, T., Wintterlin, J., Trost, J. & Ertl, G. Identification of the "active sites" of a surface-catalyzed reaction. *Science* **273,** 1688–1690 (1996).
3. Buurmans, I. L. C. & Weckhuysen, B. M. Heterogeneities of individual catalyst particles in space and time as monitored by spectroscopy. *Nat. Chem.* **4,** 873–886 (2012).
4. Ristanović, Z. *et al.* Quantitative 3D fluorescence imaging of single catalytic turnovers reveals spatiotemporal gradients in reactivity of zeolite H-ZSM-5 crystals upon steaming. *J. Am. Chem. Soc.* **137,** 6559–6568 (2015).
5. Andoy, N. M. *et al.* Single-molecule catalysis mapping quantifies site-specific activity and uncovers radial activity gradient on single 2D nanocrystals. *J. Am. Chem. Soc.* **135,** 1845–1852 (2013).
6. Bechtel, H. A., Muller, E. A., Olmon, R. L., Martin, M. C. & Raschke, M. B. Ultrabroadband infrared nanospectroscopic imaging. *Proc. Natl Acad. Sci. USA* **111,** 7191–7196 (2014).
7. Hermann, P. *et al.* Characterization of semiconductor materials using synchrotron radiation-based near-field infrared microscopy and nano-FTIR spectroscopy. *Opt. Express* **22,** 17948–17958 (2014).
8. Stavitski, E. & Weckhuysen, B. M. Infrared and Raman imaging of heterogeneous catalysts. *Chem. Soc. Rev.* **39,** 4615–4625 (2010).
9. Gross, E. *et al. In Situ* IR and X-ray high spatial-resolution microspectroscopy measurements of multistep organic transformation in flow microreactor catalyzed by Au nanoclusters. *J. Am. Chem. Soc.* **136,** 3624–3629 (2014).
10. Muller, E. A., Pollard, B. & Raschke, M. B. Infrared chemical nano-imaging: accessing structure, coupling, and dynamics on molecular length scales. *J. Phys. Chem. Lett.* **6,** 1275–1284 (2015).
11. Centrone, A. Infrared imaging and spectroscopy beyond the diffraction limit. *Annu. Rev. Anal. Chem. (Palo Alto, Calif.)* **8,** 101–126 (2015).
12. van Schrojenstein Lantman, E. M., Deckert-Gaudig, T., Mank, A. J. G., Deckert, V. & Weckhuysen, B. M. Catalytic processes monitored at the nanoscale with tip-enhanced Raman spectroscopy. *Nat. Nanotechnol.* **7,** 583–586 (2012).
13. Huth, F. *et al.* Nano-FTIR absorption spectroscopy of molecular fingerprints at 20 nm spatial resolution. *Nano Lett.* **12,** 3973–3978 (2012).
14. van Schrojenstein Lantman, E. M., de Peinder, P., Mank, A. J. G. & Weckhuysen, B. M. Separation of time-resolved phenomena in surface-enhanced Raman scattering of the photocatalytic reduction of *p*-nitrothiophenol. *ChemPhysChem* **16,** 547–554 (2015).
15. Blum, C. *et al.* Tip-enhanced Raman spectroscopy – an interlaboratory reproducibility and comparison study. *J. Raman Spectrosc.* **45,** 22–31 (2014).
16. Ayache, M., Lux, S. F. & Kostecki, R. I. R. Near-field study of the solid electrolyte interphase on a tin electrode. *J. Phys. Chem. Lett.* **6,** 1126–1129 (2015).
17. Mastel, S., Govyadinov, A. A., de Oliveira, T. V. A. G., Amenabar, I. & Hillenbrand, R. Nanoscale-resolved chemical identification of thin organic films using infrared near-field spectroscopy and standard Fourier transform infrared references. *Appl. Phys. Lett.* **106,** 023113 (2015).
18. Pollard, B., Muller, E. A., Hinrichs, K. & Raschke, M. B. Vibrational nano-spectroscopic imaging correlating structure with intermolecular coupling and dynamics. *Nat. Commun.* **5,** 3587 (2014).
19. Berweger, S. *et al.* Nano-chemical infrared imaging of membrane proteins in lipid bilayers. *J. Am. Chem. Soc.* **135,** 18292–18295 (2013).
20. Levratovsky, Y. & Gross, E. High spatial resolution mapping of chemically-active self-assembled N-heterocyclic carbenes on Pt nanoparticles. *Faraday Discuss.* **188,** 345–353 (2016).
21. Crudden, C. M. *et al.* Ultra stable self-assembled monolayers of N-heterocyclic carbenes on gold. *Nat. Chem.* **6,** 409–414 (2014).
22. Zhukhovitskiy, A. V., Mavros, M. G., Van Voorhis, T. & Johnson, J. A. Addressable carbene anchors for gold surfaces. *J. Am. Chem. Soc.* **135,** 7418–7421 (2013).
23. Rühling, A. *et al.* Modular bidentate hybrid NHC-thioether ligands for the stabilization of palladium nanoparticles in various solvents. *Angew. Chem. Int. Ed.* **55,** 5856–5860 (2016).
24. Arnold, R., Azzam, W., Terfort, A. & Wöll, C. Preparation, modification, and crystallinity of aliphatic and aromatic carboxylic acid terminated self-assembled monolayers. *Langmuir* **18,** 3980–3992 (2002).
25. García-García, F. R., Bion, N., Duprez, D., Rodríguez-Ramos, I. & Guerrero-Ruiz, A. H. $_2$/D_2 isotopic exchange: a tool to characterize complex hydrogen interaction with carbon-supported ruthenium catalysts. *Catal. Today* **259,** 9–18 (2016).
26. Janssens, T. V. W. *et al.* Insights into the reactivity of supported Au nanoparticles: combining theory and experiments. *Top. Catal.* **44,** 15–26 (2007).
27. Somorjai, G. A. & Blakely, D. W. Mechanism of catalysis of hydrocarbon reactions by platinum surfaces. *Nature* **258,** 580–583 (1975).
28. Vang, R. T. *et al.* Controlling the catalytic bond-breaking selectivity of Ni surfaces by step blocking. *Nat. Mater.* **4,** 160–162 (2005).
29. Lopez, N. *et al.* On the origin of the catalytic activity of gold nanoparticles for low-temperature CO oxidation. *J. Catal.* **223,** 232–235 (2004).
30. Kang, L. L. *et al. In situ* surface-enhanced Raman spectroscopy study of plasmon-driven catalytic reactions of 4-nitrothiophenol under a controlled atmosphere. *ChemCatChem* **7,** 1004–1010 (2015).

Acknowledgements F.D.T. thanks the Director, Office of Science, Office of Basic Energy Sciences and the Division of Chemical Sciences, Geosciences, and Biosciences of the US Department of Energy at LBNL (DE-AC02-05CH11231) for partial support of this work. We thank the M. Raschke group at the University of Colorado for collaborating on the development of the SINS endstation. The Advanced Light Source is supported by the Director, Office of Science, Office of Basic Energy Sciences, of the US Department of Energy under contract number DE-AC02-05CH11231. W.J.W. thanks the NSF for a predoctoral fellowship (DGE 1106400), and the Arnold Group (UCB) for use of their infrared spectrometer.

Author Contributions E.G. and F.D.T. conceived the idea and co-wrote the paper. C.-Y.W. and W.J.W. prepared the carbene ligands and attached them to Pt and Au surfaces. Y.L. analysed the XPS measurements. H.A.B. and M.C.M. designed the SINS beamline and assisted in conducting the SINS measurements and analysing the data. E.G. performed the SINS experiments and analysed the data. All authors contributed to the overall scientific interpretation and edited the manuscript.

Author Information Reprints and permissions information is available at www.nature.com/reprints. The authors declare no competing financial interests. Readers are welcome to comment on the online version of the paper. Correspondence and requests for materials should be addressed to E.G. (elad.gross@mail.huji.ac.il) or F.D.T. (fdtoste@berkeley.edu).

Reviewer Information *Nature* thanks C. Campbell, G. Rothenberg, F. Tao, B. Weckhuysen and the other anonymous reviewer(s) for their contribution to the peer review of this work.

METHODS

Sample preparation. Pt particles were prepared by evaporation of metallic Pt film (3 nm at a deposition rate of 0.3 nm s^{-1}) on Si(110) surface, which was coated with a native layer of SiO_2. This process was followed by annealing of the Pt-coated surface to 823 K for 5 h, leading to formation of Pt particles in the size range of 100 ± 30 nm (ref. 20). XRD measurements identified a dominant (200) facet in the particles. Cross-sectional and profile analysis of the particles was conducted using AFM measurements. The particles were 20 ± 5 nm in height, and the length of their profiles was 20 nm (Extended Data Fig. 10).

Au particles were prepared by evaporation of an equivalent of 20-nm Au film on Si(110) surface, which is coated with a native layer of SiO_2, at a deposition rate of 0.3 nm s^{-1}. This process was followed by annealing of the Au coated surface to 1,073 K for 2 h under N_2 environment to prevent coating of the metallic particle with a SiO_2 layer[31]. HR-SEM measurements verified that Au particles in the size range of 300 ± 100 nm were formed following this pretreatment (Extended Data Fig. 4).

Synthesis of OH-functionalized NHCs and their attachment to the surface. A detailed schematic of the synthesis of NHCs is provided in Extended Data Fig. 1. The preparation and activation of NHCs were performed in a glove box. The free carbene was prepared by addition of KO^tBu (3.4 mg, 0.03 mmol) to a solution of **B** (10 mg, 0.03 mmol) in THF (3 ml) and stirred at room temperature for 2.5 h (ref. 32).

The Pt-coated Si wafer was placed in a 20-ml scintillation vial in a glove box. The freshly prepared carbene solution was transferred into the vial and covered the Pt-coated Si surface. After 48 h, the Si wafer was removed from the glove box and washed three times with THF (5 ml) and distilled water (5 ml) intermittently. The sample was then flushed with N_2 for 5 min and stored in a glove box until infrared nanospectroscopy measurements were conducted.

Synthesis of NO_2-functionalized carbene molecules and their attachment to the surface. The compound was prepared according to the method in ref. 33. In the glove box, a 20-ml scintillation vial was charged with the imidazolium bromide salt (20 mg, 0.04 mmol) and THF (11 ml). A 1-dram vial was charged with lithium hexamethyldisilazide (7 mg, 0.04 mmol, 1 equiv.) and THF (1 ml). Both vials were placed into the glove box freezer (−20 °C) for 20 min, and then the LiHMDS solution was quickly added to the imidazolium bromide suspension. The vial was quickly swirled to mix, and then a 3-ml aliquot was transferred via pipette to a separate 20-ml scintillation vial containing a silica wafer with the sample of interest; four separate samples can be treated simultaneously using this method. The vials containing the silica wafers and the carbene solution were capped and placed in the glove box freezer to incubate for 24 h. After this time, the vials were removed from the glove box and the silica wafers were washed with MilliQ water and then with THF in three separate cycles. After the final wash, the carbine-treated wafers were placed in a dry 20-ml scintillation vial and dried under a stream of N_2 and stored in the glove box.

Surface characterization. Si-coated Pt and Au samples were analysed by XPS (Extended Data Figs 2 and 4, respectively). Far-field ATR-IR measurements were used to detect the properties of NHCs following their exposure to reducing and oxidizing conditions (Extended Data Fig. 3).

Synchrotron infrared nanospectroscopy. Synchrotron infrared light (provided by the Advanced Light Source, Lawrence Berkeley National Laboratory) was focused onto the apex of an oscillating Pt–Si AFM tip (Nanosensors, PtSi-NCH) at frequency ω in a modified commercial AFM (Innova, Bruker). Because the near-field scattered signal depends nonlinearly on the distance between the tip and the sample, the tip oscillation induces higher harmonics ($n\omega$) in the near-field scattered signal. As a result, the near-field signal can be differentiated from the far-field background by detecting high harmonics of frequency ω with a lock-in amplifier. In this case, the high-harmonic frequency of 2ω was detected. A modified commercial FTIR spectrometer (Nicolet 6700, Thermo Scientific) was used to collect the infrared nanospectroscopy measurements. Following AFM topography imaging of the surface, infrared nanospectroscopy point and line measurements were conducted at selected locations of the surfaces of the particles. The Fourier transform of the interferogram provides a complex-valued near-field spectrum. The real ($\mathrm{Re}(\nu)$, where ν is the wavenumber) and imaginary ($\mathrm{Im}(\nu)$) spectra can be represented as spectral amplitude ($A(\nu)$) and phase ($\varphi(\nu)$). The near-field spectra were reported either in the form of a normalized scattering amplitude ($A(\nu) = A_{\mathrm{sample}}(\nu)/A_{\mathrm{reference}}(\nu)$) or in the form of a normalized scattering phase ($\varphi(\nu) = \varphi_{\mathrm{sample}}(\nu)/\varphi_{\mathrm{reference}}(\nu)$), using the bare Si surface as a reference point.

Data availability. The data that support the plots within this Letter and the other findings of this study are available from the corresponding authors upon reasonable request.

31. Bowker, M. *et al.* Encapsulation of Au nanoparticles on a silicon wafer during thermal oxidation. *J. Phys. Chem. C* **117,** 21577–21582 (2013).
32. Jurčík, V., Gilani, M. & Wilhelm, R. Easily accessible chiral imidazolinium salts bearing two hydroxy-containing substituents as shift reagents and carbene precursors. *Eur. J. Org. Chem.* **2006,** 5103–5109 (2006).
33. Sato, T., Hirose, Y., Yoshioka, D. & Oi, S. N-heterocyclic carbenes with a *N*-2,4-dinitrophenyl substituent: comparison with PPh_3 and IPr. *Organometallics* **31,** 6995–7003 (2012).

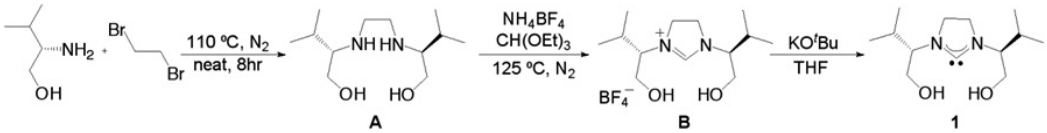

Extended Data Figure 1 | Preparation schematic of free OH-functionalized carbene. Preparation procedure of carbene **1** that was anchored to the surface of Pt particles.

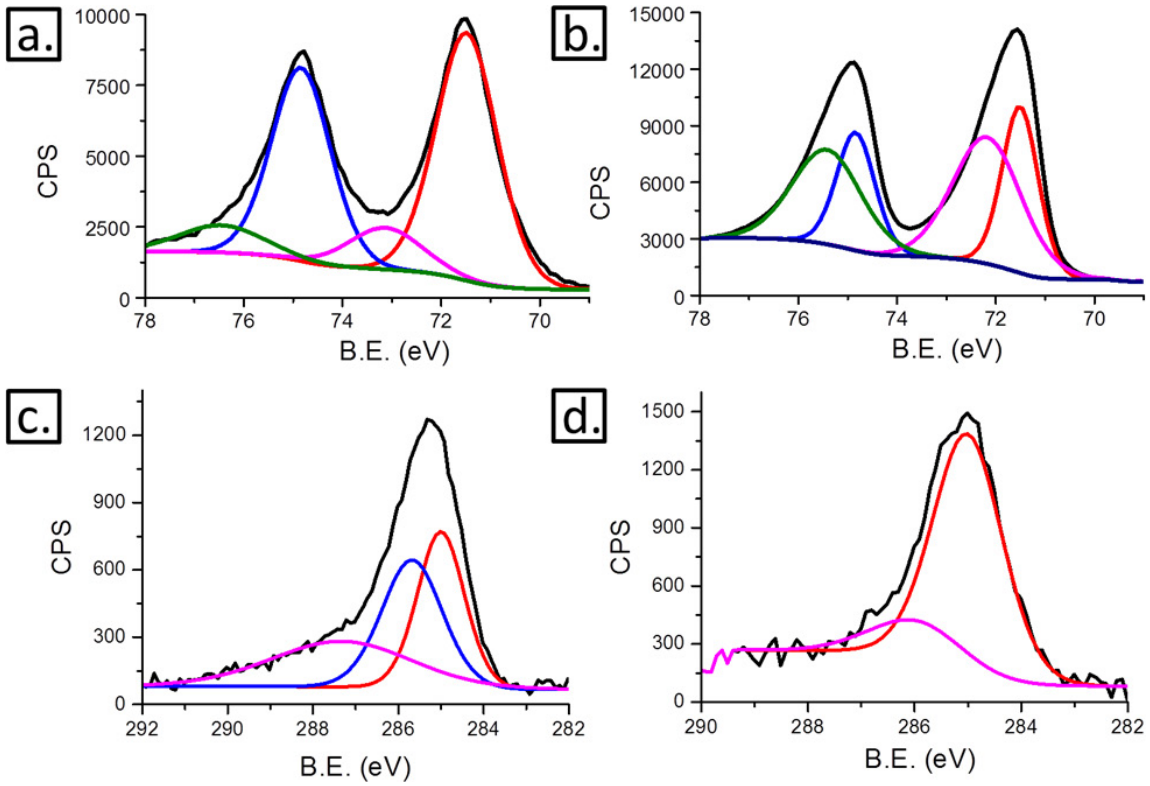

Extended Data Figure 2 | XPS measurements of Pt particles with and without NHCs. a, **b**, Pt 4*f* XPS data before (**a**) and after (**b**) the adsorption of NHCs on Pt particles. **c**, **d**, C 1*s* XPS data following exposure of the NHC-coated Pt particles to oxidizing (O_2, 70 °C, 10 h; **c**) and reducing (H_2, 70°C, 10 h; **d**) conditions. XPS data (black curves) and the calculated Gaussians that construct the measured XPS signal (coloured curves) are shown. CPS, counts per second; B.E., binding energy.

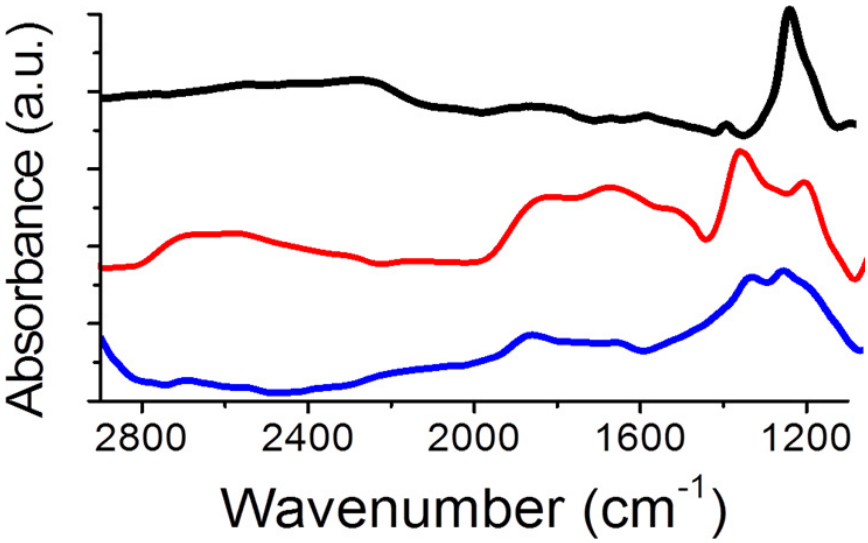

Extended Data Figure 3 | Far-field ATR-IR spectra of NHC-coated Pt particles. ATR-IR measurements were conducted after the following treatments: blue, exposure of the sample to mild oxidizing conditions (1 atm O_2, 40 °C, 10 h); red, exposure of the sample to harsher oxidizing conditions (1 atm O_2, 70 °C, 10 h); black, exposure of the sample to reducing conditions (1 atm H_2, 70 °C, 10 h).

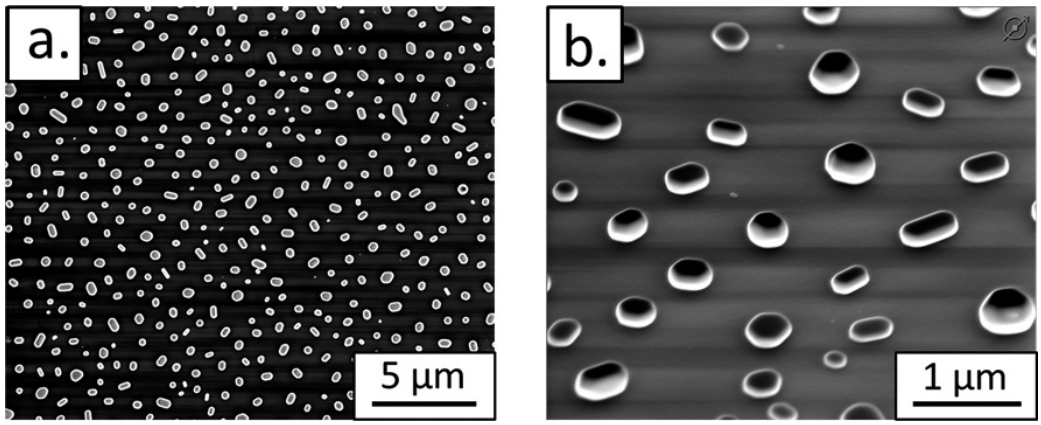

Extended Data Figure 4 | HR-SEM images of Au particles. a, **b**, Low-magnification (**a**) and high-magnification (**b**) HR-SEM images were taken following deposition of 20-nm Au film on Si(110) surface and surface annealing (under flow of N_2) to 1,073 K for 2 h.

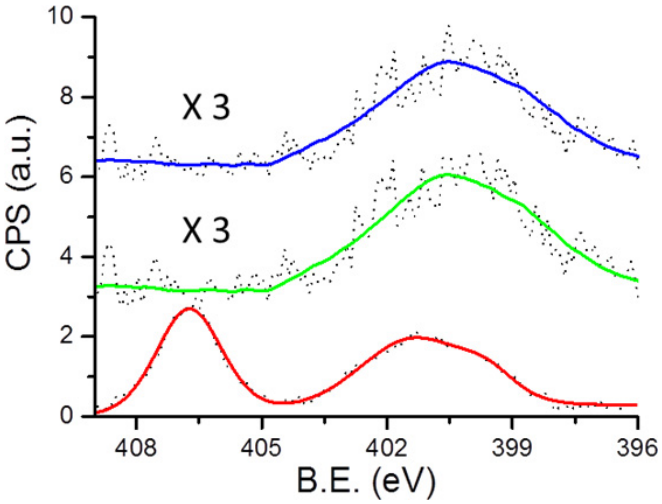

Extended Data Figure 5 | XPS measurements of Au particles coated with NO_2-functionalized NHCs. N 1*s* XPS data of NO_2-functionalized NHCs that were attached to the surface of Au particles. XPS measurements were conducted before (red spectrum) and after the exposure of the sample to reducing environment, using $NaBH_3CN$ (green spectrum) or $NaBD_3CN$ (blue spectrum) as a reducing agent. The black dots represent the measured XPS data points; the coloured curves are the averaged XPS signals. The XPS signals that were measured after exposure of the sample to reducing agents (blue and green spectra) have been multiplied by three.

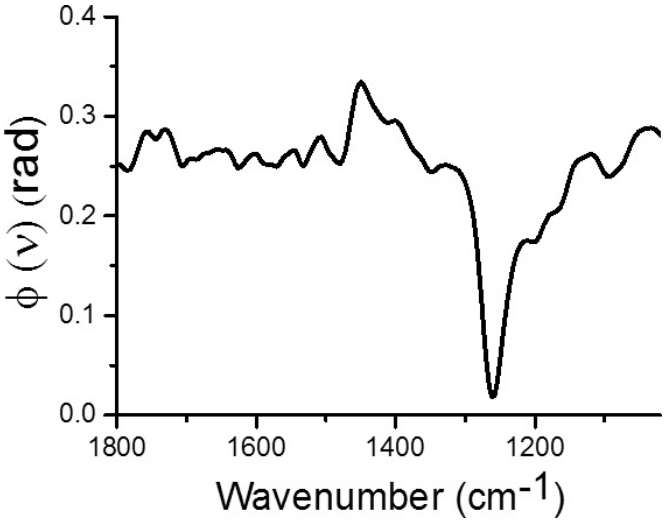

Extended Data Figure 6 | Full SINS spectrum of Au particles coated with NO_2-functionalized NHCs. NHCs were attached to the surface of Si-supported Au particles. The sample was exposed to reducing conditions with a deuterated reagent. The dip in the scattering signal around 1,250 cm^{-1} is induced by a high Si signal from the reference spectra.

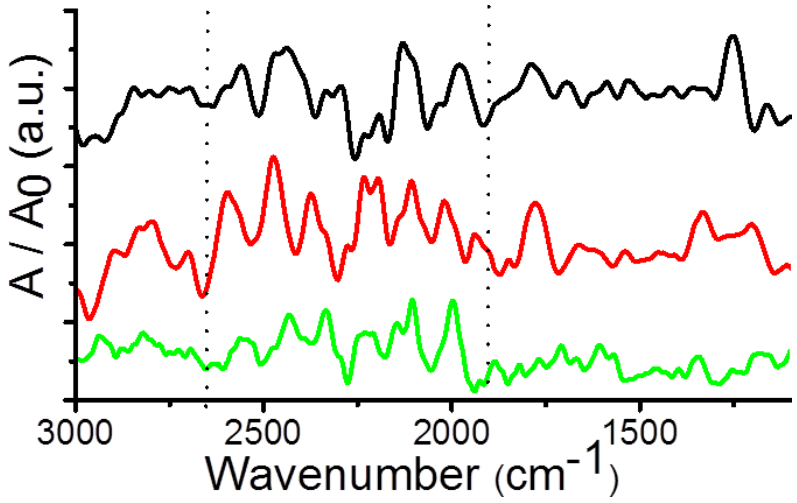

Extended Data Figure 7 | Full spectra of the SINS point measurements. Infrared point measurements were conducted on the bare Si surface (green spectrum) and on the edge and centre of a single Pt particle (red and black spectra, respectively). High noise levels between 1,900 cm^{-1} and 2,600 cm^{-1} (indicated by the vertical dotted lines) are induced by the presence of a diamond window that separates the ultrahigh-vacuum part of the light source from the rough vacuum area and that highly absorbs the infrared light in this range.

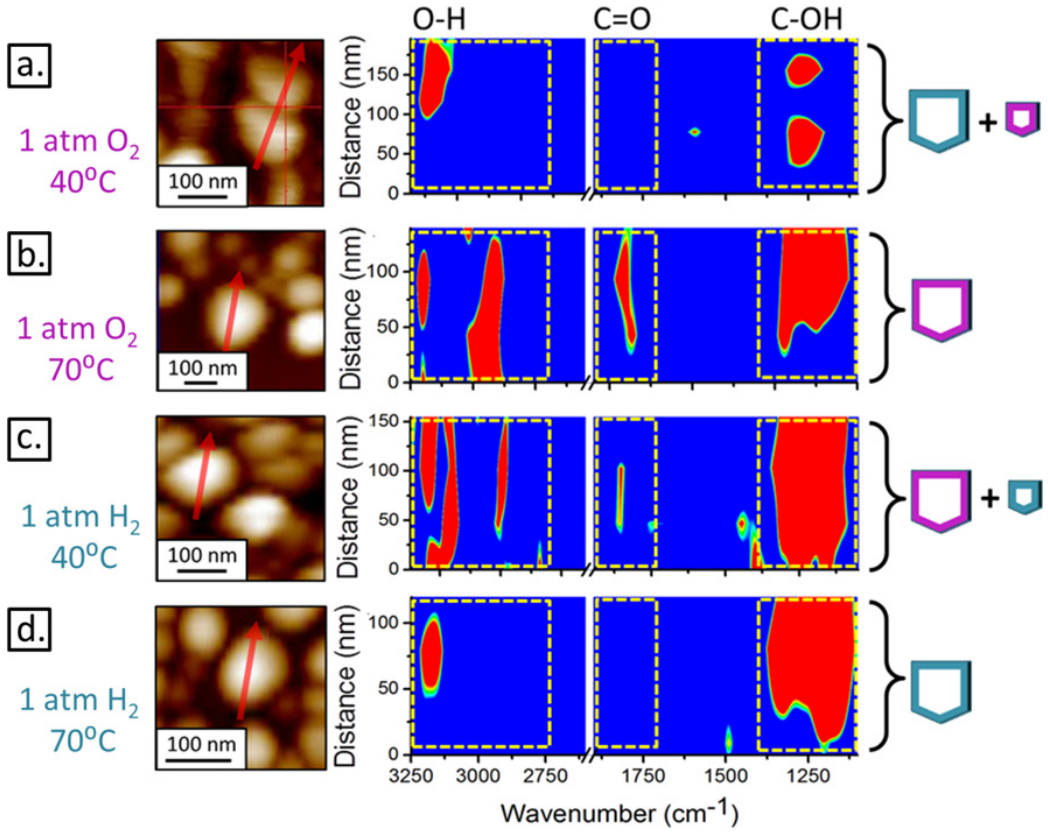

Extended Data Figure 8 | Non-biased spectra of SINS line-scan measurements. The corresponding biased spectra are shown in Fig. 3. **a**–**d**, AFM topography scans and infrared nanospectroscopy line scans were conducted following exposure of the sample to various oxidizing (**a**, **b**) and reducing (**c**, **d**) conditions. The path of the infrared line scans along the surface is marked by red arrows in the AFM images (left). The colour and size of the different pentagons represent the chemical properties and surface densities of NHCs, as detected by the infrared line scans (blue, OH functional group; purple, acid functional group). The relatively narrow O–H peaks at high wavenumbers are correlated to a deteriorated signal-to-noise ratio in this region. Because only the most dominant part of the O–H peak is highlighted in this colour scheme, the peak width is reduced to about 250 wavenumbers.

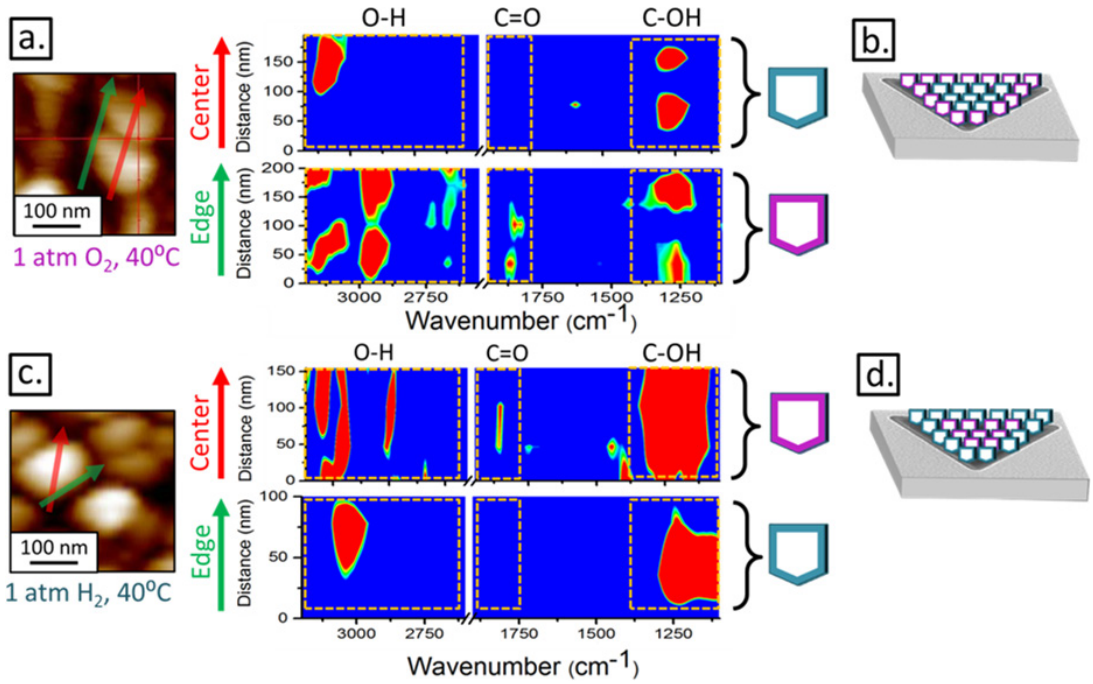

Extended Data Figure 9 | Non-biased spectra of SINS line-scan measurements. The corresponding biased spectra are shown in Fig. 4. Infrared nanospectroscopy line scans were performed across the centre and edge of NHC-coated Pt particles (marked by red and green arrows, respectively, in the AFM images). **a**, **c**, Infrared nanospectroscopy measurements were conducted after the samples were exposed to mild oxidizing (**a**) and reducing (**c**) conditions. The coloured pentagons (blue, OH functional group; purple, acid functional group) represent the molecules that reside on the centre and edge of the particle as detected by infrared line-scan measurements. The relatively narrow O–H peak of the carboxylic acid was correlated to a deteriorated signal-to-noise ratio at high wavenumbers. Because only the most dominant part of the O–H peak is highlighted in this colour scheme, the peak width is about 250 wavenumbers. **b**, **d**, Schematics of Pt particles with NHCs (coloured pentagons) following their exposure to oxidizing (**b**) and reducing (**d**) conditions.

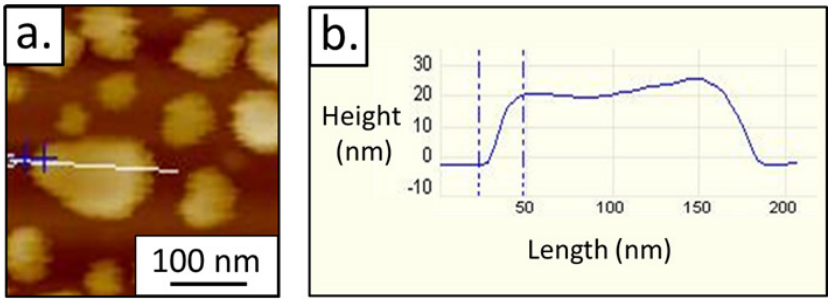

Extended Data Figure 10 | Cross-sectional analysis of NHC-coated Au particles. a, AFM topography image of NHC-coated Pt particles that were deposited on Si surface. The white line indicates the path of the line scan along the sample. **b**. Cross-sectional analysis of the height of one Pt particle. The length of the profile of the particle is about 20 nm (indicated by the distance between the vertical dash-dotted lines; the positions of which are indicated by blue crosses in **a**). The error in the AFM height measurements is about 2%, as estimated by measurements of the roughness of the surface of the particle.

Author Queries

Journal: **Nature**
Paper: **nature20795**
Title: **High-spatial-resolution mapping of catalytic reactions on single particles**

Query Reference	Query
1	AUTHOR: This PDF proof has been produced on the basis of your corrections to the preproof and contains the main-text figures edited by us and the Extended Data items supplied by you (which may have been resized but will not have been edited otherwise by us). Please check that the display items are as follows (doi:10.1038/nature20795): Figs 1–5 (colour); Tables, none; Boxes, none; Extended Data display items, 10 figures. Please check the edits to all main-text figures very carefully, and ensure that any error bars in the figures are defined in the figure legends. If you wish to revise the Extended Data items for consistency with main-text figures and tables, please copy the style shown in the PDF proof (such as italicising variables and gene symbols, and using initial capitals for labels) and return the revised Extended Data items to us along with your proof corrections.
2	AUTHOR: Please define the uncertainty here and elsewhere, for example as standard deviation or standard error.
3	AUTHOR: Please mention the dashed boxes in **e** and **f** as well.
4	AUTHOR: The newest version of this figure did not contain any pentagons; should it have done?
Web summary	The chemical conversion of N-heterocyclic carbene molecules attached to catalytic particles is monitored at high spatial resolution using synchrotron-radiation-based infrared nanospectroscopy.

For Nature office use only:

Layout	☐	Figures/Tables/Boxes	☐	References	☐
DOI	☐	Error bars	☐	Supp info	☐
Title	☐	Colour	☐	Acknowledgements	☐
Authors	☐	Text	☐	Author contribs	☐
Addresses	☐	Methods	☐	COI	☐
First para	☐	Received/Accepted	☐	Correspondence	☐
		AOP	☐	Author corrx	☐
		Extended Data	☐	Web summary	☐
				Accession codes link	☐
				Referee accreditation	☐

SUBJECT WORDS
Physical sciences/Chemistry/Catalysis/Heterogeneous catalysis [URI /639/638/77/887];Physical sciences/Chemistry/Surface chemistry/Surface spectroscopy [URI /639/638/542/971];Physical sciences/Chemistry/Catalysis/Catalytic mechanisms [URI /639/638/77/885].

TECHNIQUE TERMS
Not Applicable.